Structural, Magnetic, and Optical Properties of Orthoferrite Thin Films

by

William Wagner Supplee, Jr.

Submitted to the Department of Materials Science and Engineering
in partial fulfillment of the requirements for the degree of

Bachelor of Science in Materials Science and Engineering

at the

MASSACHUSETTS INSTITUTE OF TECHNOLOGY

June 2007

Author .....
Department of Materials Science and Engineering
May 22, 2007

Certified by .....
Caroline Ross
Professor of Materials Science and Engineering
Thesis Supervisor

Accepted by .....
Caroline Ross
Chairman, Undergraduate Thesis Committee

Structural, Magnetic, and Optical Properties of Orthoferrite Thin Films

by

William Wagner Supplee, Jr.

Submitted to the Department of Materials Science and Engineering
on May 22, 2007, in partial fulfillment of the
requirements for the degree of
Bachelor of Science in Materials Science and Engineering

Abstract

Pulsed laser deposition was used to create thin films of Ce-Fe-O and Y-Fe-O systems. Deposition temperature and ambient oxygen pressure were varied systematically between samples to determine which deposition conditions were most favorable to the formation of cerium/yttrium orthoferrite. The structure and composition of each film were then determined using X-ray diffraction and wavelength dispersive spectroscopy respectively. In addition, the magnetic and optical properties of the yttrium films were characterized to determine the suitability of these materials as Faraday isolators at λ=1550 nm. Results show that orthoferrite crystal structures in these systems are not stable in the temperature and oxygen ranges tested. It was also found that increasing oxygen pressure caused exponential decay in the deposition rate. Most films were amorphous, exhibiting a paramagnetic M-H plot and a Verdet coefficient between 0.37 and 0.89 deg cm^{-1} $Gauss^{-1}$.

Thesis Supervisor: Caroline Ross
Title: Professor of Materials Science and Engineering

Acknowledgments

There are several people without whom my research would not have been possible. Among them, I would like to thank Lei Bi, Alex Taussig, and Professor Caroline Ross for their advice, guidance, and assistance in the lab. I learned a great deal about life in the laboratory from them and am grateful for the experience. I would also like to thank Matthew Handler, Vladimir Tarasov, and F. Gene Shuman for their assistance during a very busy academic year.

THIS PAGE INTENTIONALLY LEFT BLANK

Contents

List of Figures

THIS PAGE INTENTIONALLY LEFT BLANK

List of Tables

THIS PAGE INTENTIONALLY LEFT BLANK

Chapter 1

Introduction

The basic mangetooptical materials currently used in the near infrared region are iron garnets [1]. They are popular for their relatively high Faraday effect coupled with their extremely low attenuation in the near infrared region [2]. As technology advances, a suitable Faraday isolator that can be grown epitaxially on Si or InP becomes increasingly attractive for microphotonic applications. Unfortunately, the iron garnet has a lattice constant that is more than twice that of silicon [3], rendering growth of these crystals in microphotonic applications difficult due to the large lattice mismatch. As a result, there is a renewed interest in orthoferrite thin films, which have desirable properties similar to the iron garnet, but with a lattice constant closer to Si and InP. These orthoferrites have been fabricated since 1950, when their magnetic properties were first characterized [4]. Data on the optical and magnetic properties of these materials is abundant. A review of this early research was conducted by White in 1966. [11].

To this end, the fabrication of epitaxial yttrium orthoferrite and cerium orthoferrite was investigated. The goal was to systematically determine deposition conditions (i.e. substrate temperature and ambient O_2 pressure) to yield the desired orthoferrite crystal reproducibly. Thickness and roughness measurements were conducted Furthermore, the M-H loops and Verdet constants of the yttrium orthoferrite thin films were to be quantitatively characterized and compared to accepted values in the literature. The eventual aim of this work is to establish base deposition conditions

for more complex orthoferrite structures, such as double metallic orthoferrites (for example, $La_{1-x}Bi_xFeO_3$).

Chapter 2

Theoretical Background

The remaining chapters assume a basic familiarity with fundamental concepts in materials science. However, there are two principles that must be understood in greater detail to understand the implications of this work.

2.1 Orthoferrites

2.1.1 Crystal Structure

Orthoferrites are compounds with formula $RFeO_3$, where R is often a rare earth or transition metal. Their structure is to the first order that of the perovskites [4], the chemical formula for which takes on the general form ABO_3. Thus, orthoferrites are essentially perovskites in which the B-site is occupied by Fe. An example of a common cubic perovskite at room temperature is $BaTiO_3$; its unit cell is shown in Figure 2-1.

The unique magnetooptical properties of orthoferrites are a direct consequence of their structure. This will be explained in 2.1.2. For now, it is important to note that which makes most commonly studied orthoferrites special is their unit cell is slightly orthorhombic instead of cubic like $BaTiO_3$. Indeed, the orthoferrite unit cell is very nearly cubic as in fig 2-1, but instead the angle between the c-axis and the a-b plane is slightly greater than 90 degrees [4]. This orthorhombic cell manifests itself as a slight canting in the unit cell of the orthoferrite – usually on the order of 0.6° [4, 6].

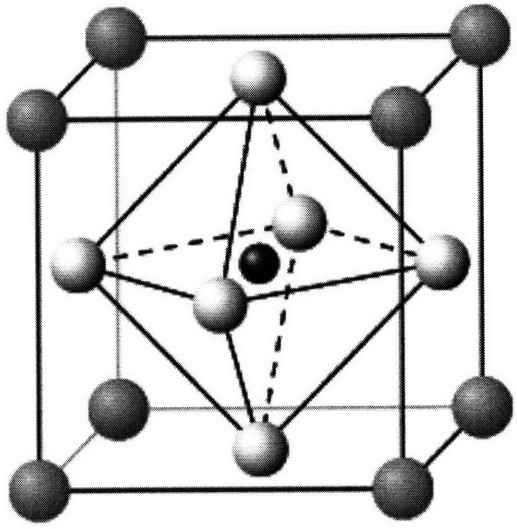

Figure 2-1: $BaTiO_3$, a typical cubic perovskite. The corner atoms are Ba, the face atoms are O, and the octahedrally "trapped" atom is Ti. Source: [5]

2.1.2 Magnetic and Optical Properties

As previously mentioned, the slight canting of the unit cell in many orthoferrites, especially $YFeO_3$, is largely responsible for their magnetic and optical characteristics. In fact, the typical arrangement of magnetic moments in the Fe sublattice is antiparallel, resulting in an antiferromagnetic material [5]. Thankfully, the slight canting of the unit cell in $YFeO_3$ is enough to cause the material to respond as a weak ferrimagnet, producing a net magnetic moment of 0.04 - 0.05 μ_B molecule^{-1} [7]. The strong antiparallel alignment of Fe magnetic moments also results in films with an extremely high coercivity. Indeed, the strong dipole coupling in the ferrimagnet results in effective "pinning" of the magnetized state. Consequently, $YFeO_3$ films with coercivities as high as 8 kG have been reported [4]! The M-H loop of a $YFeO_3$ sample is shown in figure 2-2. The empirical M_{sat} value for $YFeO_3$ is around 8 emu/cm^3 [4, 8].

In terms of optical properties, $YFeO_3$ is considered the most transparent of the orthoferrites in the near infrared range [9]. Figure 2-3 shows the optical absorption spectrum for $YFeO_3$ as a function of wavelength. $YFeO_3$ also exhibits a specific Faraday rotation that is slightly higher than that of yttrium iron garnet (YIG), as shown in figure 2-4. However, YIG possesses about one-tenth the attenuation of

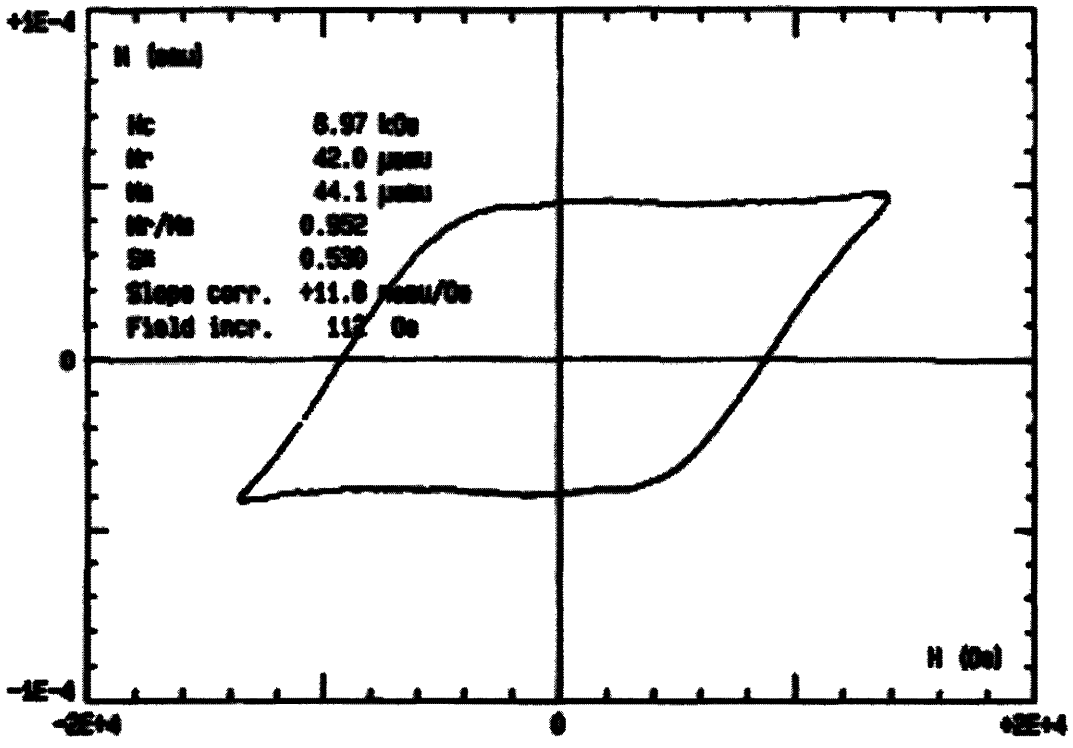

Figure 2-2: The perpendicular M-H loop of a $YFeO_3$ thin film taken with the alternating gradient force magnetometer. The loop has been corrected for the substrate contribution. Source: [4]

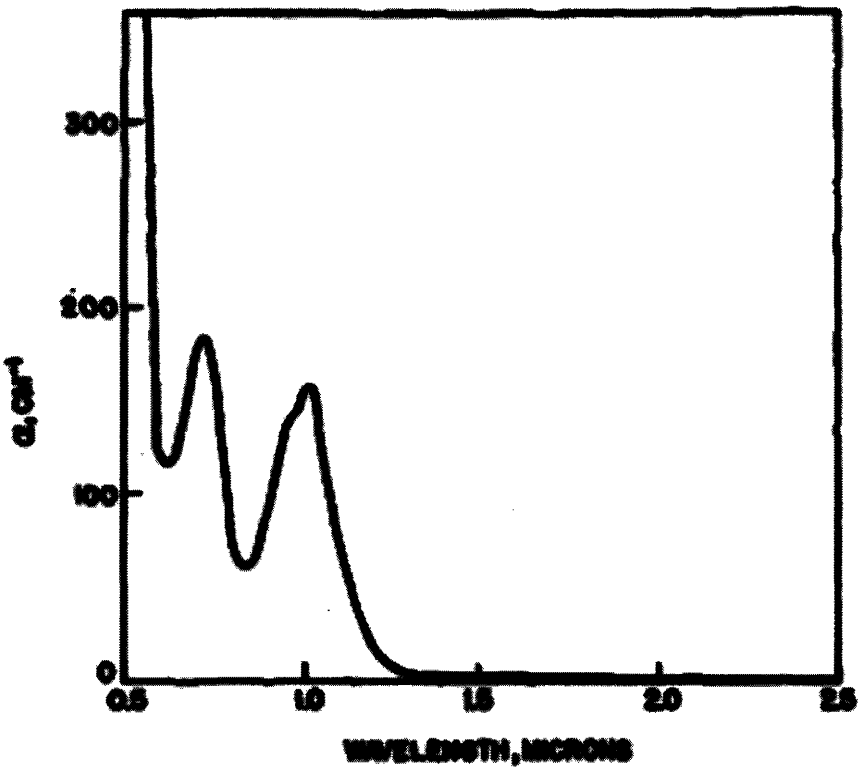

Figure 2-3: Absorption spectrum for $YFeO_3$. Note the extremely low attenuation at both λ=1300 nm and λ=1550 nm. Source: [9].

$YeFeO_3$ in the near IR range, ultimately giving YIG a higher figure of merit (FOM).

2.2 The Faraday Effect

2.2.1 Qualitative Treatment

The main motive for the renewed interest in orthoferrite thin films revolves around their potential use as lattice-matched Faraday isolators in microphotonic circuits. The ability of these films to function in this capacity is a result of their pronounced Faraday effect. H. R. Hulme describes the Faraday effect qualitatively in *Proceedings of the Royal Society of London*: "If plane polarised light be transmitted through a medium under the influence of a magnetic field parallel to the direction of propagation, the plane of polarisation is in general rotated" [10]. Of particular interest is that rotation

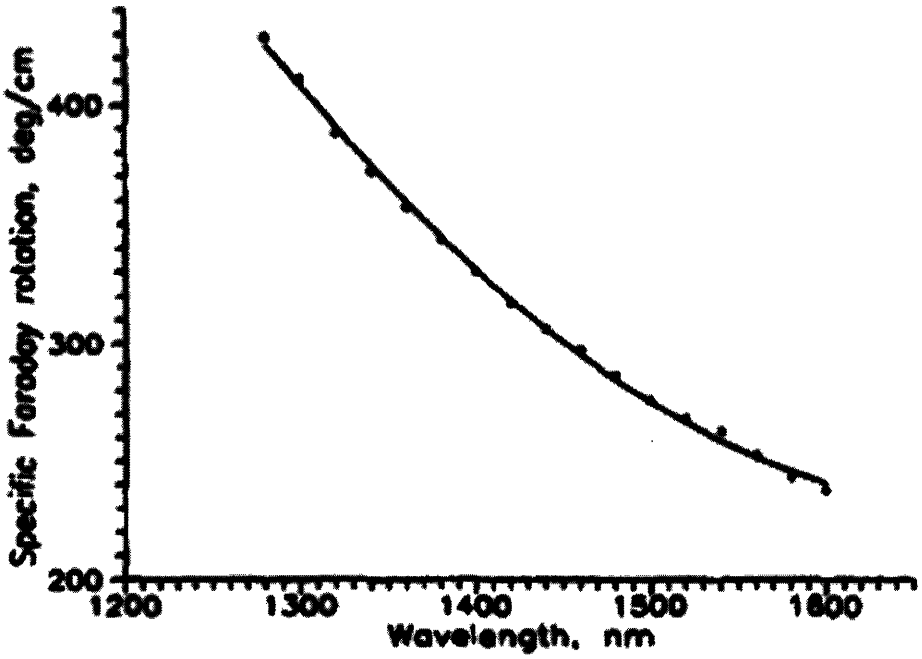

Figure 2-4: Faraday rotation in yttrium orthoferrite versus wavelength. Source: [1].

of the plane of polarization is not reciprocal – that is to say the plane is rotated in the same direction regardless of the direction of propagation. Thus, a material that rotates light of a given wavelength by 45° coupled with a plane polarizer could act as a Faraday isolator.

Faraday rotation, however, is dependent on the thickness of the sample, the magnitude of the applied field, and the wavelength of light. The intrinsic material quantity that relates thickness and applied field to the Faraday rotation for a given wavelength is known as the Verdet constant. Because this quantity is intrinsic, it is often more useful in comparing Faraday rotation between materials. The equation that relates the Verdet constant to the applied field and film thickness is

$$\beta = BVd$$

[10], where β is the amount of Faraday rotation (in degrees), B is the applied field, V is the verdet constant, and d is the material thickness (most frequently in centimeters).

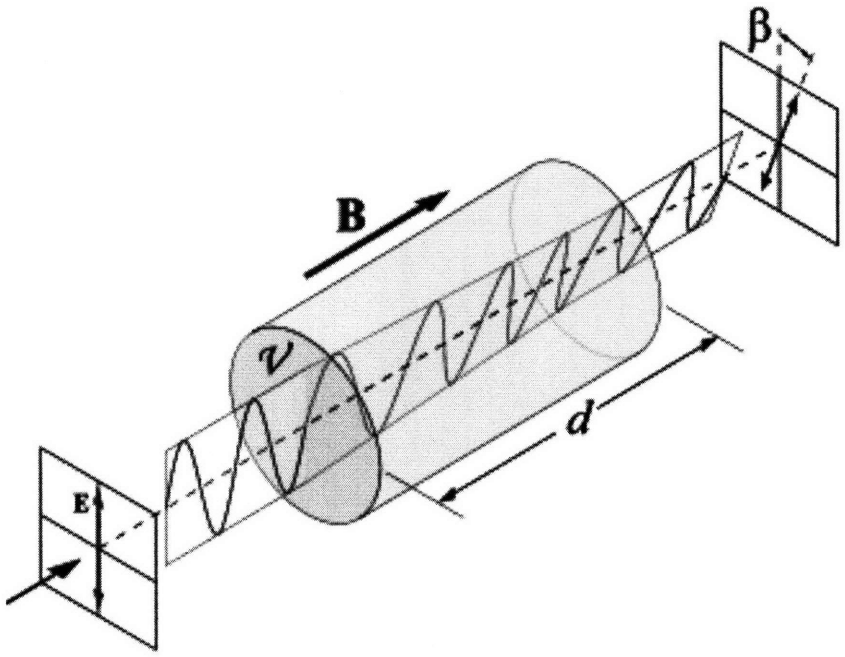

Figure 2-5: A theoretical depiction of Faraday rotation in a material.

This physical meaning of this equation is shown in figure 2-5.

Chapter 3

Structural Properties of Ce-Fe-O Thin Films

3.1 Deposition Conditions

Deposition of the Ce-Fe-O thin films was carried out via pulsed laser deposition (PLD), also known as pulser laser ablation (PLA). Pulsed laser deposition is essentially an evaporative deposition process, and deposition therefore normally occurs at very low ambient pressures. Our deposition was conducted with an ambient chamber pressure of less than 10^{-6} Torr. The chamber was pumped down in two stages: first with a rough pump, then by a turbopump. Once this vacuum threshold was achieved, ambient oxygen (p_{O_2}) was permitted to flow into the chamber prior to deposition. While many parameters can be controlled in this process, the two most essential are the substrate temperature (T_s) and the oxygen pressure (p_{O_2}). Several samples were fabricated, each at a different combination of substrate temperature and oxygen partial pressure. Thus, the structural properties of each sample could be characterized in a matrix according to the deposition conditions. The summary of these deposition conditions is found in Table 3.1.

Table 3.1: PLD parameters for Ce-Fe-O film deposition.

Control Variable	Value
T_s	500°C, 700 °C
p_{O_2}	0.001, 0.5, 1, 5, 50 mTorr
λ	248 nm (KrF)
E	550 mJ
f	10 Hz
P	5.5 W
Target Ce:Fe	0.88:1
Substrate	MgO(001), Si(001)

3.1.1 Deposition Rate

Naturally, because the ambient gas pressure was varied between depositions, the mean free path varied as well, thereby changing the total deposition rate (in nm kilopulse^{-1}). The effect of p_{O_2} on the deposition rate was investigated. The result is Figure 3-1. Note the rather large error bars (some as large as ±20%). This is a result of the imprecise film thickness measurements described in Section 3.2.2. Also, because of the large number of control variables that had to be fixed in order to make this comparison, there are only a small set of (6) data points. Nonetheless, the points appear to weakly outline an exponential plot, with possible outliers near $p_{O_2} = 0.001$ mTorr.

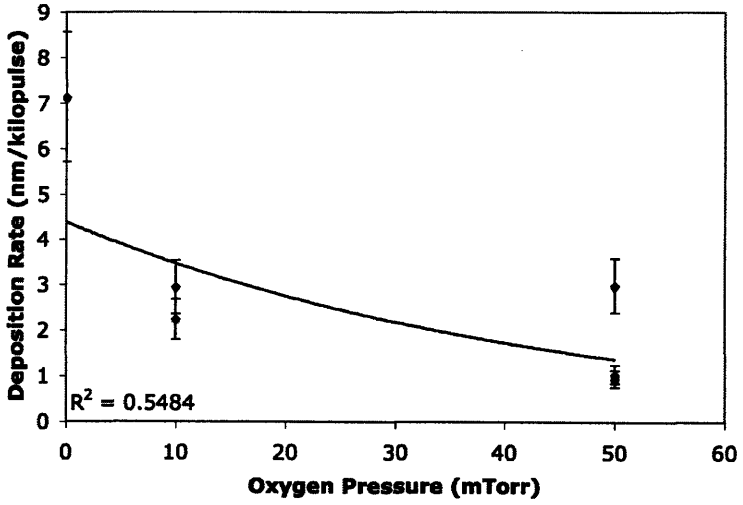

Figure 3-1: The effect of p_{O_2} on deposition rate

3.2 Film Characterization

3.2.1 Crystallinity and Stoichiometry

Crystalline phases in MgO films were identified by Lei Bi via 2DXRD. 2DXRD scans both the conventional Bragg angle in X-ray diffractometry, θ, as well as the angle in the orthogonal plane, ϕ. [12]. This is particularly useful for films of varying composition. Because XRD is such a fundamental structural analysis tool in materials science, and because the author did not directly take these measurements, a detailed description of the process is omitted. Information on both XRD and 2DXRD can be found in [12] and [13].

The stoichiometry (Ce:Fe) of the MgO films was determined using Wavelength Dispersive Spectroscopy (WDS), performed by Lei Bi and Dr. Nilanjan Chatterjee. WDS measures the intensity of emitted photons that are generated when valence electrons fall into lower energy states. These lower energy states are vacated by the ejection of core electrons from atoms in the sample. The instrument outputs radiation intensities at different wavelengths. These intensities were converted into at. % by the author using standard software, thus determining the stoichiometric ratio of Ce:Fe in the film.

The result of these measurements is found in 3.2.

3.2.2 Thickness and Roughness Measurements

Thickness measurements were taken on these samples using a Tencor P10 Surface Profilometer with a 2 μm radius diamond stylus on the Si (001) samples. The Si (001) substrate samples were fabricated simultaneously with corresponding MgO (001) samples at the same deposition conditions. The Si samples were also half covered by a Si mask during deposition, so that profilometry measurements showed a sharp "step" in each sample. This height of this step was recorded as the effective film thickness. The profilometry tip traced a 1.6 mm line, starting 1.2 mm from the step, and ending 0.4 mm across the bare Si substrate. The tip was centered on the sample to estimate the

film thickness at the sample center. This measurement was repeated twice, at ±10% from the center of the sample, to account for lack of uniformity in film thickness. The Tencor P10 software also reported an RMS roughness for the film.

The result of these measurements is found in 3.3.

3.3 Results

3.3.1 Film Phases and Stoichiometry

Table 3.2: Ce-Fe-O film phases and stoichiometry as a function of the deposition conditions. If no crystal structure is listed, the film was found to be amorphous. The stoichiometry is written as Ce:Fe.

$p_{O_2}(mTorr)$	T_s = 500°C	T_s = 700°C
0.001	1.17	1.28, poly CeO_2, hematite
0.5	1.060	1.070
1	1.159, amorphous CeO_2	1.169, CeO_2 (111)
5	1.358, CeO_2 (111)	1.232, CeO_2 (111)
50	1.891, CeO_2 (100)	1.662, CeO_2 (100)

As Table 3.2 shows, no orthoferrites were grown at these substrate temperatures or oxygen pressures. In general, a greater atomic percentage of cerium is found in these films as the oxygen pressure is increased. Also, the film tended to crystallize as the film stoichiometry deviated from 1. Possible reasons for these trends and the lack of orthoferrite phases are discussed in Chapter 5.

3.3.2 Film Thickness and Roughness

Table 3.3: Ce-Fe-O film thickness as a function of the deposition conditions.

$p_{O_2}(mTorr)$	T_s = 500°C	T_s = 700°C
0.001	204 ±4 nm	313 ±15 nm
0.5	166 ±33 nm	190 ±14 nm
1	393 ±4 nm	401 ±8 nm
5	360 ±19 nm	405 ±5 nm
50	204 ±36 nm	207 ±9 nm

It is clear that profilometry is a rough estimate of the film thickness at best. In some samples the standard deviation approaches 20%. Because this data was used to determin deposition rate, the plot in section 3.1.1 has a very low R^2 value. Better alternatives to profilometry in determining film thickness are discussed in Chapter 5. The Tencor P10 software reported the RMS roughness for each sample to be under 1 nm, with the exception of the film deposited at base pressure and 700°C. This film exhibited an RMS roughness of 16 nm.

THIS PAGE INTENTIONALLY LEFT BLANK

Chapter 4

Properties of Y-Fe-O Thin Films

4.1 Film Deposition

The apparatus for film deposition in the yttrium is nearly identical to that of the cerium system. See section 3.1 for details on the pulsed laser deposition apparatus. Yttrium films, however, were deposited at different substrate temperatures (T_s) and oxygen pressures (p_{O_2}). A summary of the PLD deposition conditions for this system can be found in Table 4.1.

Table 4.1: PLD parameters for Y-Fe-O film deposition.

Control Variable	Value
T_s	400°C, 700 °C
p_{O_2}	0.001, 10, 50 mTorr
λ	248 nm (KrF)
E	550 mJ
f	10 Hz
P	5.5 W
Target Y:Fe	1:1
Substrate	MgO(001), Si(001)

4.2 Characterization Methods

The structural characterization methods (phases, stoichiometry, thickness) of these films were identical to those of the cerium system. For information on these methods,

please see the relevant section in Chapter 3.

4.2.1 Film Crystallinity and Stoichiometry

See 3.2.1.

4.2.2 Film Thickness

See 3.2.2. Roughness measurements were not taken on these films.

4.2.3 Magnetic Characterization

The magnetic hysteresis loops of the Y-Fe-O thin films were measured using a vibrating sample magnetometer (VSM). The specific VSM used was Model 1660 by ADE Technologies. VSM is a fairly common technology in magnetic characterization, and has been used since about 1960 [14]. In VSM, the sample is magnetized by two electromagnets and then vibrated between two pickup coils. The vibration of the magnetized sample causes a change in magnetic flux which induces a voltage in the coil. This concept is known as Faraday's law of induction. The VSM is calibrated to convert pickup voltage into magnetization in emu.

VSM measurements were taken for each sample to determine how the magnetization varied as a function of applied field ($H = -10^4$ - 10^4 Gauss). The applied field was stepped in intervals of 200 Gauss between -2000 to 2000 Gauss, and was stepped by intervals of 500 Gauss everywhere else.

The result of these measurements can be found in Figure 4-2.

4.2.4 Extraction of Verdet Constant

The Verdet constant, V, of each sample was determined using a custom-built apparatus designed by Dr. David C. Bono, a research scientist at MIT. A full description can be found in [15]:

Faraday rotation was measured to an accuracy of 1 mdeg using a custom-built apparatus. Collimated laser light of 1.55 μm wavelength was focused through a rotating stage consisting of a polarizer prism and a Faraday cell modulator. The incoming light was modulated by an AC signal from a lock-in amplifier. The laser light then passed through a path bored in the pole pieces of an electromagnet, between which the sample was placed. A second prism detected the modulated AC signal. In all experiments, the Faraday rotation was measured with both the applied field and the laser beam perpendicular to the plane of the film.

The result of this data collection is shown in Figure 4-1. The Verdet constant could then be determined for each material using software written by the author. The software finds the linear slope near zero rotation for all samples using the MATLAB polyfit() function, and divides the slope by the sample thickness in centimeters. The result is the Verdet constant in deg cm^{-1} $Gauss^{-1}$.

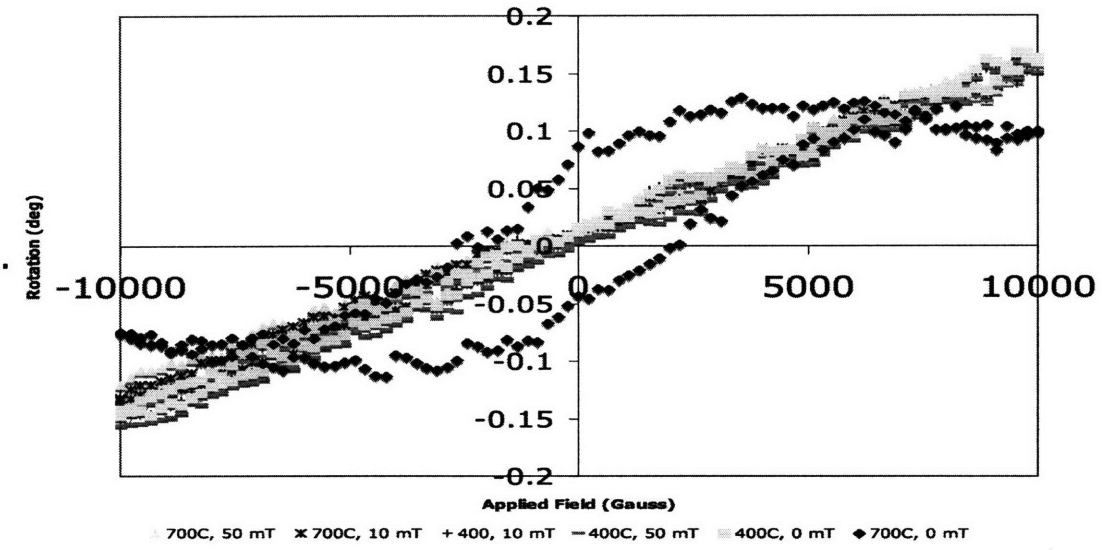

Figure 4-1: Output of the custom-built Faraday rotation apparatus for the Y-Fe-O films.

4.3 Results

4.3.1 Film Phases and Stoichiometry

Table 4.2: Y-Fe-O film phases and stoichiometry as a function of the deposition conditions. If no crystal structure is listed, the film was found to be amorphous. The stoichiometry is written as Y:Fe.

$p_{O_2}(mTorr)$	$T_s = 400°C$	$T_s = 700°C$
0.001	0.60	0.57, poly Y_2O_3, magnetite
10	0.52	0.49
50	0.49	0.41, CeO_2 (111)

Of particular interest here is the rather low stoichiometry and the prevalence of amorphous films under all tested conditions except at base pressure with T_s =700°C. No orthoferrites were formed. Possible explanations for the lack of orthoferrite phase can be found in Chapter 5.

4.3.2 Film Thickness

Table 4.3: Y-Fe-O film thickness as a function of the deposition conditions.

$p_{O_2}(mTorr)$	$T_s = 400°C$	$T_s = 700°C$
0.001	240 ±8 nm	285 ±30 nm
10	224 ±6 nm	295 ±23 nm
50	180 ±13 nm	168 ±9 nm

The data shows that deposition rate appears to decay with increasing partial pressure (although not conclusively). This will be discussed in greater detail in Chapter 5. Furthermore, thickness tended to decrease as the samples were deposited. Ideally this should not occur; this phenomenon will be discussed in Chapter 5.

4.3.3 Magnetic Characterization

Note that all films, except the film containing magnetite, are paramagnetic. The film containing magnetite exhibits a strong ferromagnetic M-H loop, which is expected. Note that the diamagnetic M-H response of the MgO substrate was measured. This

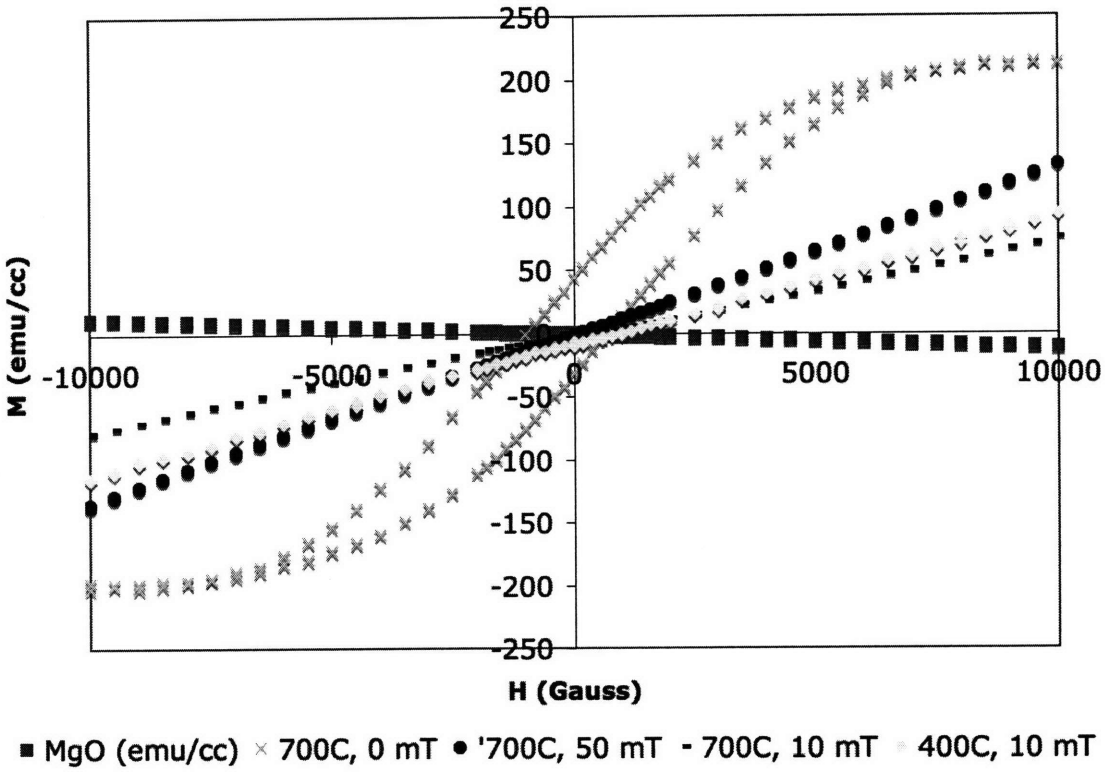

Figure 4-2: M-H plot for the Y-Fe-O films.

measurement allowed successful subtraction of the magnetic contribution of the substrate from the Y-Fe-O samples.

4.3.4 Verdet Constant

Table 4.4: Verdet constants at $\lambda = 1550$nm for the Y-Fe-O films as a function of the deposition conditions. All values are in deg cm^{-1} Gauss^{-1}.

$p_{O_2}(mTorr)$	$T_s = 400°C$	$T_s = 700°C$
0.001	0.80	0.86
10	0.89	0.34
50	0.79	0.60

Because most films lack long-range order, there appears to be no trend in the Verdet constant as a function of p_{O_2} or T_s. Based upon this data and Figure 4-1, the only possible candidate material for a Faraday isolator is the magnetite-containing film. However, as will be discussed in Chapter 5, this is not a feasible choice for a

Faraday isolator.

Chapter 5

Discussion

5.1 Fabrication of Orthoferrite Thin Films

As Tables 4.2 and 3.2 show, the orthoferrites $CeFeO_3$ and $YFeO_3$ are not stable phases at the deposition conditions chosen. This is most apparent in $CeFeO_3$. Crystalline phases only form at our deposition conditions when the atomic ratio of cerium to iron is far from 1 ($>\approx 1.15$), suggesting a perovskite structure is not energetically favorable at the chosen substrate temperatures. Literature suggests increasing the deposition temperature in order to fabricate orthoferrites. Indeed, research into phase equilibria of the Ce-Fe-O system at various temperatures and oxygen pressures was conducted extensively by Tretyakov et. al in 1976 [16]. Figure 5-1 shows all stable phases between 727 and 1327°C, and between 10^{-17} and 760 Torr.

The figure clearly shows that at $p_{O_2} = 10^{-6}$ atm, which corresponds to 1 mTorr, a substrate temperature of around 980° is necessary before polycrystalline $CeFeO_3$ can be grown. The substrate thermocouple in our system indicated that the maximum T_s achievable was 710°C for our particular apparatus, which explains why formation of the orthoferrite phase was not possible. Figure 5-1 also shows that the stable crystalline phase near 727°C is CeO_2. Indeed, Table 3.2 shows we frequently witnessed the formation of CeO_2 , at 700°C. Unfortunately, figure 5-1 does not contain data on low temperatures low enough to shed light on the data for $T_s = 500$°C. It has also been shown, however, that oxygen pressures larger than 5 mTorr damage the

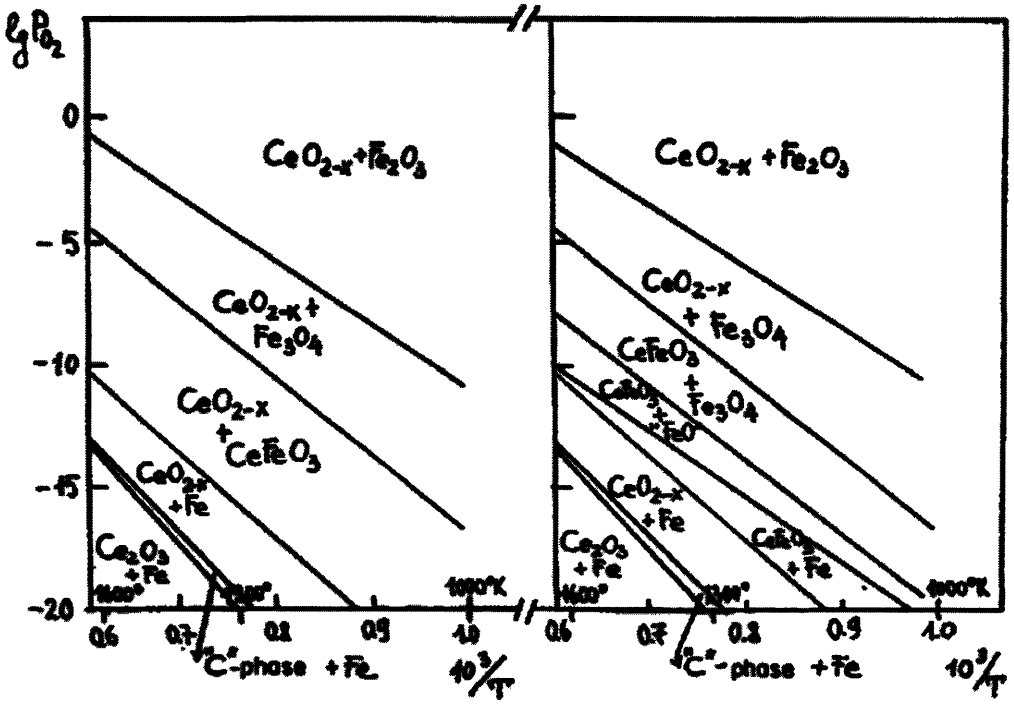

Figure 5-1: State diagram of log $P_{O_2}(atm) = f(10^3/T)(K^{-1})$ for the equilibrium mixture of condensed phases of the Ce-Fe-O system. The case where Ce:Fe > 1 is shown in (a). [16]

orthoferrite phase [16]. Therefore it is unlikely $CeFeO_3$ will form at temperatures below about 980°C using PLD.

This is similarly true in the case of $YFeO_3$. Krishnan et. al fabricated $YFeO_3$ films using a nearly identical PLD setup [4]. They reported that $YFeO_3$ were most stable when $T_s = 750°C to 900°C$ and $p_{O_2} = 10 to 50$ mTorr. It is therefore understandable that no $YFeO_3$ thin films were observed at the deposition conditions tested. In order to fabricate yttrium orthoferrite, these experiments should be repeated with T_s increased to the stable range reported in [16].

5.2 Effect of p_{O_2} on Deposition Rate

Figure 3-1 shows the relationship between increasing oxygen pressure and exponential decay of the deposition rate. There exists literature to justify the inverse proportional-

ity of oxygen pressure and deposition rate. It has been established that an increase in p_{O_2} results in a decrease in film deposition rate in pulsed laser deposition [18, 16, 20]. This is likely due to the decrease in molecular mean free path (λ) with increasing p_{O_2} (p), according to the equation [19]:

$$\lambda = \frac{\sqrt{2}}{2\pi d^2}\frac{k_B T}{p}$$

The mean free path explanation also explains why films deposited above base pressure were all very smooth: the increased collision frequency results in slower adsorption to the substrate surface, allowing more time for surface diffusion and hence a smoother film. Thus for constant substrate temperature, T_s, this effect on deposition rate as a function of p_{O_2} is expected. In fact, sources also cite the deposition rate as a function of p_{O_2} to decay exponentially, as was found in this case [18, 20]. There has been some debate about the validity of this trend, and Tyunina et. al have revealed that the effect of p_{O_2} on deposition rate varies depending on the X-ray fluence regime [21]. For low X-ray fluence, the deposition rate is linear to -log p_{O_2}. For large X-ray fluence, increasing p_{O_2} slightly from vacuum increases the total film growth rate to a certain maximum point by creating collisions that reduce the kinetic energy of ablated material, decreasing the desorption rate. Increasing the ambient gas pressure beyond this critical amount then causes exponential decay of the film growth rate again [21].

Research suggests that many of the controllable PLD chamber conditions heavily influence the film deposition rate [17, 18, 21]. Such conditions include, but are not limited to: the distance between the source and substrate, the substrate temperature, the X-ray fluence, and pulse frequency. Therefore, in order to perform an accurate analysis of the effect of p_{O_2} on deposition rate, all of these other factors including substrate temperature had to be held constant. For this reason, there are only six data points in figure 3-1. Further depositions at constant T_s should therefore be carried out to better determine the nature of the decay in deposition rate as a function of p_{O_2} strictly. Also, due to the rough measurements of thickness made by profilometry (see section 3.2.2), The accuracy of the deposition rate at each data point is guaranteed

to within only 20%. A combination of more deposition data points with ellipsometry for determining film thickness is recommended for further research.

5.3 Magnetic and Optical Properties of Y-Fe-O Films

With the exception of the film forming magnetite crystals, all of the thin films fabricated at the tested deposition conditions exhibit paramagnetic behavior. This is likely due to the lack of long-range order in the films, which subsequently affects their ability to form "permanent" magnetic domains. Indeed, the octahedral Fe sites in $YFeO_3$ have made it a popular structure for the study of magnetic domain walls [4], as the antiferromagnetic alignment of the Fe ions creates pinned domain structures. Consequently, $YFeO_3$ films have remarkably low M_{sat} (8 emu/cc) and remarkably large coercivities – sometimes as large as 9 kG [4]. So while it may be difficult to resolve the magnetization of successfully fabricated $YFeO_3$ films, the unusually large coercivity of these materials should manifest itself in figure 4-2, were any orthoferrite phases present.

The sample containing magnetite has an $M_s = \approx 225$ emu/cc, which is about half that of the bulk value for magnetite [22]. The magnetization, however, is calculated per unit volume, and the WDS data suggests that this film is only about 50% magnetite by volume. Therefore the discrepancy of about a factor of two in the magnetite film's magnetization is justified and expected.

The Verdet constants for these materials range from 0.37 deg cm^{-1} $Gauss^{-1}$ to 0.89 deg cm^{-1} $Gauss^{-1}$. However, due to the inaccurate profilometry thickness measurement technique used in this experiment (see section 3.2.2), each of these values was determined using a film thickness with a standard deviation of around 20%! This error obscures any trend in the Verdet constant data, and indeed one is not observed in table 4.4. Nevertheless, the sample possessing the highest Verdet constant also happens to be the sample containing magnetite. Indeed, heavily ferromagnetic mate-

rials are known for their particularly large magneto-optical Kerr effect and Faraday effect. These materials are stilll poor candidates for Faraday isolators, as too much light is absorbed by these materials to be feasible for photonic applications. Indeed, magnetite has an absorption coefficient of 10^5 cm^{-1} at $\lambda = 1550nm$ [23]. This value is several order of magnitudes higher than the respective absorption coefficients for both yttrium iron garnet and yttrium orthoferrite. Therefore, unfortunately, no candidate materials for Faraday isolators in microphotonic circuits were identified as a direct result of this work.

THIS PAGE INTENTIONALLY LEFT BLANK

Chapter 6

Conclusion

The goal of this work was to use pulsed laser deposition (PLD) to fabricate cerium and yttrium othroferrite thin films. To this end, the deposition temperature and ambient oxygen pressure were varied systematically between depositions to determine which deposition conditions were most favorable to the formation of these orthoferrite phases. Unfortunately, no orthoferrites were formed at the substrate temperatures and ambient oxygen pressures chosen. Research into possible reasons for this lack of orthoferrite phase suggest the most probable solution lies in increasing the substrate temperature, T_s, upon deposition. Future work should investigate the fabrication of cerium orthoferrite between 1000 and 1200°C at ambient oxygen pressures between 0.001 and 5 mTorr. Similarly, future attempts to fabricate yttrium orthoferrite should aim for target substrate temperatures, T_s, between 750 and 900°C, with ambient oxygen pressures between 10 and 50 mTorr. To eliminate the large degree of uncertainty surrounding the thickness measurements, traditional mechanical measurements by profilometry should be replaced with more accurate optical measurements via ellipsometry.

Deposition rate for these films was shown to decay exponentially as a function of ambient oxygen pressure, but the exponential curve fit poorly, and these measurements should be repeated in future work. Specifically, the relationship between ambient oxygen pressure, deposition rate, and X-ray fluence should be elucidated. Furthermore, measurements to this effect must be absolutely certain that all other

deposition conditions are held constant or the trend will be obscured.

Bibliography

[1] Y. S. Didosyan, V. Y. Barash. Faraday effect in yttrium orthoferrite in the range 1280-1600 nm. *Journal of Magnetism and Magnetic Materials.* 151(1), 1995.

[2] A.V. Antonov, A. I. Agranovskaya, G. P. Petrova, and A. G .Titova. Optical properties of yttrium-iron garnet. *Journal of Applied Spectroscopy.* 11(4), 1969.

[3] M. A. Gilleo, S. Geller. Magnetic and crystallographic properties of substituted Yttrium-Iron Garnet, $3Y_2O_3xM_2O_3(5\text{-}x)Fe_2O_3$. *Phys. Rev.* 110(1). 1958.

[4] R. Krishnan, A. Lisfi, M. Guyot, V. Cagan. Preparation and some properties of pulsed laser deposition $YFeO_3$ films. *Journal of Magnetism and Magnetic Materials.* 147(1). 1995.

[5] E. C. Dann. $MgCNi_3$ perovskite (image). http://www.chemsoc.org/chembytes/ezine/images/2001/ 2001.

[6] D. S. Schmool, N. Keller, M. Guyot, R. Krishnan, M. Tessier. Evidence of very high coercive fields in orthoferrite phases of PLD grown thin films. *Journal of Magnetism and Magnetic Materials.* 195(1), 1999.

[7] D. Treves. *J. Appl. Phys.* 36 (1965) 1033.

[8] D. S. Schmool, N. Keller, M. Guyot, R. Krishnan, and M. Tessier. Magnetic and magneto-optical properties of orthoferrite thin films grown by pulsed-laser deposition. *Journal of Applied Physics.* 86(10). 1999.

[9] D. L. Wood, J. P. Remeika, E. D. Kolb. Optical Spectra of Rare-Earth Orthoferrites. *Journal of Applied Physics.* 41(13). 1970.

[10] H. R. Hulme. *Proceedings of the Royal Society of London. Series A, Containing Papers of a Mathematical and Physical Character.* 135(826), p. 237-257. 1932.

[11] R. L. White. *Journal of Applied Physics.* 40, p. 2760. 1969.

[12] B. B. He, U. Preckwinkel, K. L. Smith. Fundamentals of two-dimensional x-ray diffraction. *Advances in X-ray Analysis.* 43:273-280, 2000.

[13] R. Jenkins and R. L. Snyder. *Introduction to X-ray Powder Diffractometry.* John Wiley & Sons, Inc., New York, NY, 1996.

[14] S. Foner. Versatile and sensitive vibrating sample magnetometer. *Review of Scientific Instruments*, 30:548-557, 1959.

[15] A. Rajami, G. F. Dionne, D. Bono, and C. A. Ross. Faraday rotation, ferromagnetism, and optical properties of Fe-doped $BaTiO_3$. *Journal of Applied Physics*, 98:063907-1-063907-4, 2005.

[16] Yu. D. Tretyakov, V. V. Sorokin, A. R. Kaul, A. P. Erastova. Phase equilibria and thermodynamics of coexisting phases in rare-earth element-iron-oxygen systems: The cerium-iron-oxygen-system. Journal of Solid State Chemistry. 18(3), p. 253-261. 1976.

[17] J. S. Ha, G. Y. Sung, S. Lee, Y. R. Jang, K. H. Yoo, C. H. Bae, et. al. The effects of ambient oxygen pressure on the 1.54 μm photoluminescence of Erdoped silicon-rich oxide films grown by laser ablation of a Si + Er target. *Journal of Applied Physics A.* 79(4), p 1485-1488. 2004.

[18] Bohdan Kotlyarchuk, Victor Savchuk. Application of laser beam technology for preparation of oxide thin films. *CAOL 2003*, p. 149-150. September 16-20, 2003.

[19] C. A. Ross. Vacuums. *3.155/6.152J Lectures.* Lecture 6, slide 3. 2007.

[20] Can Wang, B. L. Cheng, S. Y. Wang, H. B. Lu, Y. L. Zhou, Z. H. Chen, G. Z. Yang. Effects of oxygen pressure on lattice parameter, orientation, surface

morphology, and deposition rate of $(Ba_{0.02}Sr_{0.98})TiO_3$ thin films grown on MgO substrate by pulsed laser deposition. *Thin Solid Films.* 485, p. 82-89. 2005.

[21] M. Tyunina, J. Levoska, S. Leppavuori. *Journal of Applied Physics.* 83, p. 5489. 1998.

[22] X. Liu, T. Nagai, F. Itoh. Magnetic and magneto-optical properties of Fe/Fe_3O_4 multilayers prepared by pulsed laser deposition. *Journal of Magnetism and Magnetic Materials*, 2002.

[23] A. Schlegel, S. F. Alvarado, and P. Wachter. Optical properties of magnetite (Fe_3O_4). *J. Phys. C: Solid State Phys.* 12, p. 1157-1164. 1979.